Electronic Supplementary Information: **High Broadband Photoconductivity of few-layered MoS_2 Field-effect Transistor Measured in Multi-terminal Method: Effect of Contact Resistance**

Priyanka Das[1], Jawnaye Nash[1], Micah Webb[1], Raelyn Burns[1], Varun N. Mapara[2], Govinda Ghimire[1], Daniel Rosenmann[3], Ralu Divan[3], Denis Karaiskaj[2], Stephen A. McGill[4], Anirudha V. Sumant[3], Qilin Dai[1], Paresh C. Ray[1], Bhausaheb Tawade[5], Dharmaraj Raghavan[5], Alamgir Karim[6] and Nihar R. Pradhan[1,4]

[1]Layered Materials and Device Physics Laboratory,Department of Chemistry, Physics and Atmospheric Science,Jackson State University, Jackson, MS 39217, USA
[2]Department of Physics, University of South Florida, Tampa, USA
[3]Center for Nanoscale Materials, Argonne National Laboratory, 9700 S-Cass Avenue, Lemont, IL-60439, USA
[4]National High Magnetic Field Laboratory, Tallahassee, FL 32310, USA
[5]Department of Chemistry, 6525 College Street, NW, Howard University, Washington DC 20059, USA
[6]Department of Chemical & Biomolecular Engineering, University of Houston,S333 Engineering Bldg 1, 4726 Calhoun Rd, Houston, TX 77204, USA

1. Raman characterizations:

Raman study was carried out for single layer, 4-layers, 7 layers and bulk MoS_2 crystals using a Renishaw inVia Raman setup at oxygen environment after exfoliating the flakes from the bulk single crystal.

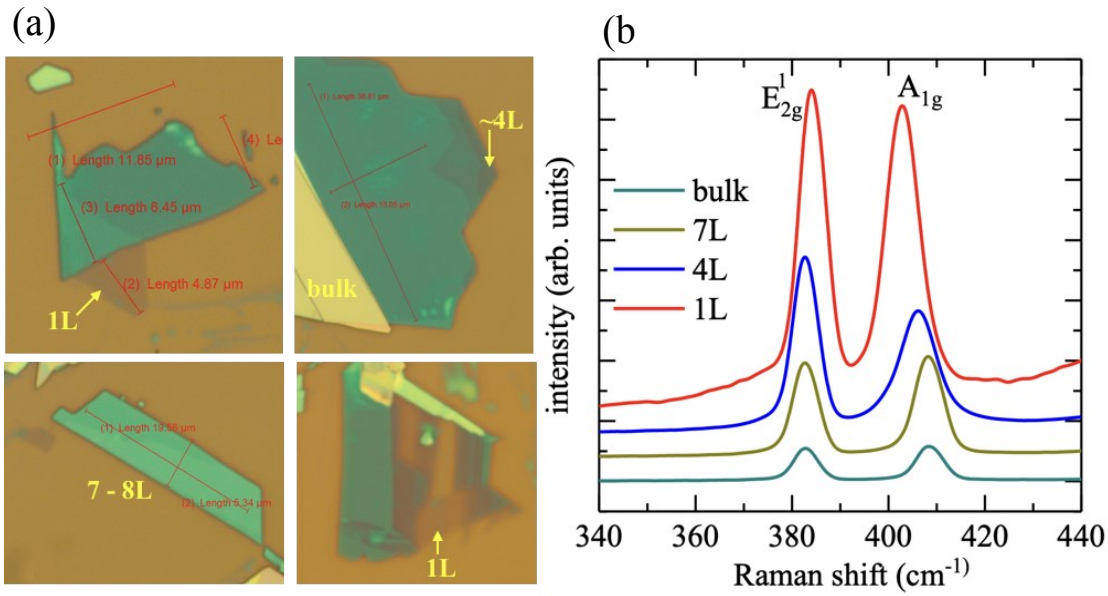

Figure S1: (a) Optical images of MoS_2 flakes of 1L, 4L, 7L and bulk single crystal exfoliated on to the Si/SiO_2 substrate measured at room temperature in oxygen atmosphere. (b) displays the Raman spectrum for 1L- bulk.

Figure S1(a) shows the exfoliated flakes on 285 nm thick SiO_2 deposited on Si substrate. Single layer MoS_2 shows E^1_{2g} peaks at 384 cm^{-1} and A_{1g} at 403 cm^{-1} and the difference between the peak position is 19 cm^{-1}. The Raman peaks for 4L crystal are at 382.6 cm^{-1} and 406 cm^{-1} for E^1_{2g} and A_{1g} modes respectively with the difference between them is 23.4 cm^{-1}. Similarly, the bulk MoS_2 shows the E^1_{2g} and A_{1g} peaks are at 382.7 cm^{-1} and 408.4 cm^{-1} respectively. All these peak positions match well with previously reported values [18].

2. Photocurrent comparison between 2- and 4-terminal methods

The photocurrent is calculated by subtracting the dark current (without elimination) from the current measured through both 2- and 4-terminal methods under white light illumination at given power by using the relation $I_{ph} = I_{light} - I_{dark}$. Figure S2 shows a photocurrent plot of 2- and 4-terminal measurements using an incident power $P_{opt} = 2.27$ nW, which shows enhancement of the photocurrent in 4-terminal method. The enhancement is much more pronounced in the ON state of the transistor, compared to that in its OFF state.

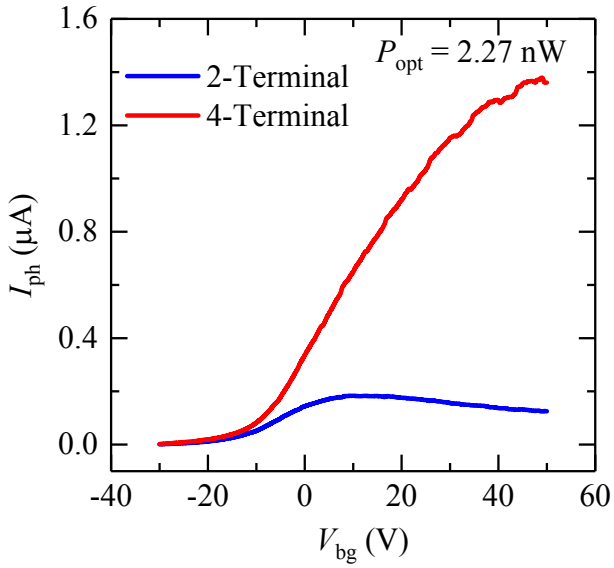

Figure S2: Comparison of photocurrent of the MoS_2 phototransistor measured in 2- and 4-terminal configuration under white light illumination at applied V_{ds} = 0.2 V and power P_{opt} = 2.27 nW.

Table-1: Comparison of phototransport parameters of several reported MoS_2 phototransistors

Materials	**Wavelength (nm)**	**R (AW^{-1})**	**Bias (V)**	**Optical Power**	**D*(Jones)**	**PDCR**	**EQE (%)**	**Ref.**
MoS2-1 L	450	0.0075	7	80 µW	-	-	-	1
MoS_2	450-633	0.05-0.12	1	50 mW/cm^2	10^{10}-10^{11}	-	-	2
MoS2-1 L	561	880	8	24 µW/cm^2	-	-	-	3
MoS_2	532	0.57	10	2 ×10^4 W/cm^2	10^{10}	10	-	4
MoS_2 (Gr contact)	400-600	1 × 10^4	1	0.1 mW/cm^2	-	-	-	5
MoS_2	466	2.48 × 10^2	1	6-30 mW/cm^2	-	-	-	6
MoS_2 (73 L)	445	0.0507	10	8 mW	1.55 ×10^9	-	-	7
MoS_2 (APTES doped)	655	56.5	5	5.8 mW/cm^2	4.47 × 10 ^{9}	-	-	8
MoS_2 (local V_{bg})	532	342.6	1	2 mW/cm^2	-	-	-	9
MoS_2	532	59	1.2	1.69 mW/cm^2			13.8×10^2	10
MoS_2/HfO_2	635	10^4	5	3.2 mW/cm^2	8 x 10^{13}	-	-	11
MoS_2/Si	808	0.9082	-2	1.69 mW/cm^2	1.889 x 10^{13}	-	-	12
MoS_2/Si	808	0.3	0	1 mW/cm^2	1 x 10^{13}	-	-	13
MoS_2/Si	365	7.2-2	-2	4 mW/cm^2	10^9	-	-	14
MoS_2/Gr	635	5 x 10^8	0.1	6.4 fW µm^{-2}	-	-	-	15
MoS_2/Gr	632.8	62	1	0.22 mW/cm^2	-	-	-	16
MoS_2-HZO	637	96.8	0.5	2.7 nW	4.75×10^{14}	-	1.88×10^4	17
MoS_2 (few layers)	400-900	**2T:** 10^3(400nm), 5 (900nm) **4T:** 10^4(400nm), 5 (800nm)	0.2	0.02 nW (0.03 mW/cm^2)	**2T:** 7x10^{10}(400nm) 5 x 10^9 (900nm) **4T:** 10^{11} (400nm) 5 x 10^9 (900nm)	**2T:** 50 (400nm) 5 (900nm) **4T:** 90 (400nm) 5 (900nm)	**2T:** 10^3, 10 **4T;** 10^6, 10	**This Work**

3. Responsivity vs Optical power: Power Law Fit

Figure S3 (a) and S3 (b) depicts the power law fit $R \propto P_{opt}^{-\gamma}$ to the responsivity vs optical power data described in the Fig. 3 in the main text. From the fitting, we obtained the exponent γ = 0.5-0.6 for both 2- and 4-terminal measurements.

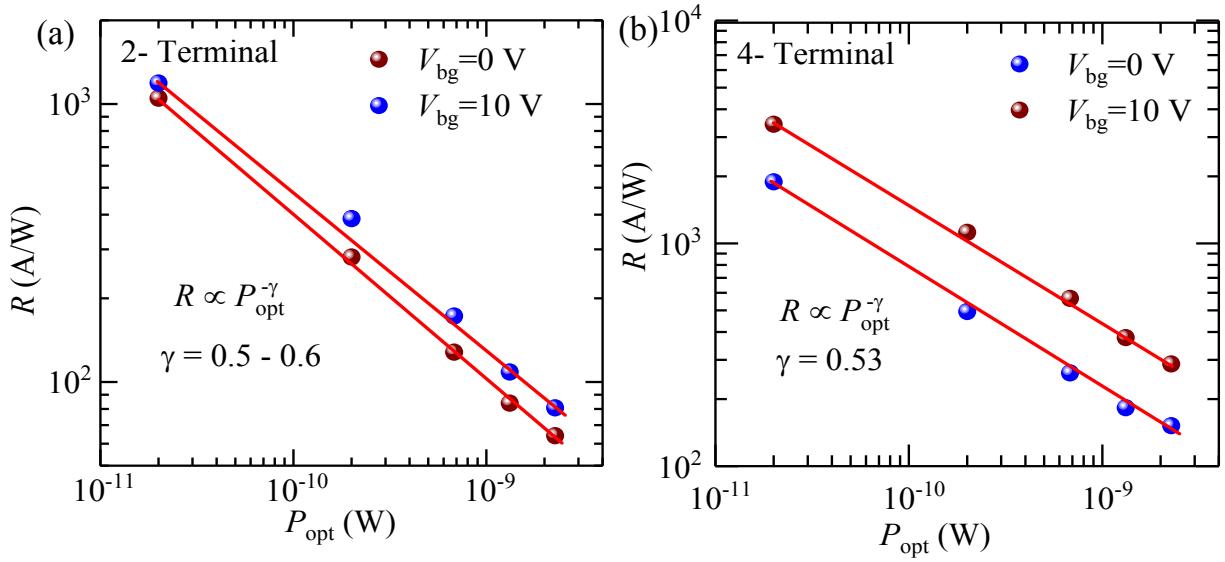
(a)
2- Terminal
V_{bg}=0 V
V_{bg}=10 V
$R \propto P_{opt}^{-\gamma}$
γ = 0.5 - 0.6
R (A/W)
P_{opt} (W)
(b)
4- Terminal
V_{bg}=0 V
V_{bg}=10 V
$R \propto P_{opt}^{-\gamma}$
γ = 0.53
R (A/W)
P_{opt} (W)

Figure S3: (a) and (b) Display the responsivity as a function of P_{opt} in logarithmic scale extracted from 2-terminal and 4-terminal measurements, respectively. Blue dots and dark red color are the data for applied gate voltages V_{bg} = 0V and 10 V respectively. The solid lines are the power law fits to the experimental data.

4. External Quantum efficiency

The external quantum efficiency (EQE) was extracted using the following relation

$$EQE = R\frac{hc}{\lambda q}$$

Where R is the responsivity, h is plank's constant, q is the electron charge and λ is the wavelength. Figure S3 (a) and S3 (b) shows the EQE values, measured using 2- and 4-terminal configuration, as a function of back gate voltage at various incident wavelengths (400 nm to 900 nm).

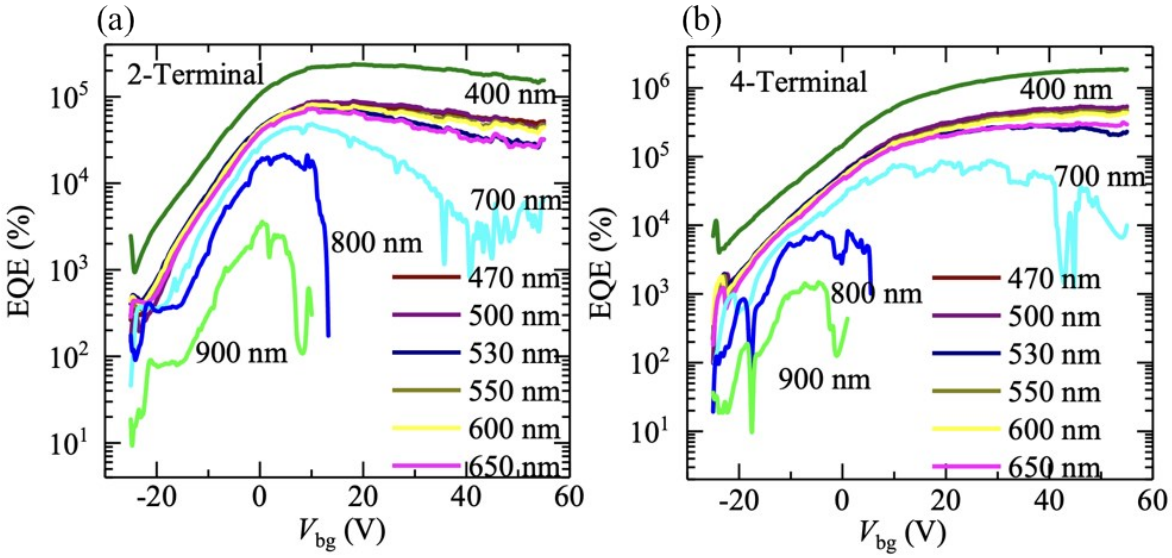

Figure S4: External quantum efficiency (EQE) values for the MoS_2 device presented in the main text measured using monochromatic light at different wavelengths in two (Figure S3 (a) and four (Figure S3 (b)) -terminal configurations.

The highest EQE value measured using the 2-terminal method was in the order of 10^5 % when the applied gate voltage V_{bg} = 10 V and V_{ds} = 0.2 V under the monochromatic light of wavelength λ =

400 nm. The maximum EQE value decreases in IR region to 10^3 % at λ = 900 nm. When the device operated in 4-terminal configuration, the EQE value increases to 10^6 % at λ = 400 nm which is an order of magnitude higher than the values obtained from 2-terminal measurements, due to the elimination of contact resistance.

Results from MoS_2 device # 2

5. FET characteristic

We measured the FET characteristic of a second device and the electrical properties I_{ds} vs V_{ds} and I_{ds} vs V_{bg} are plotted in the Figure S5 below.

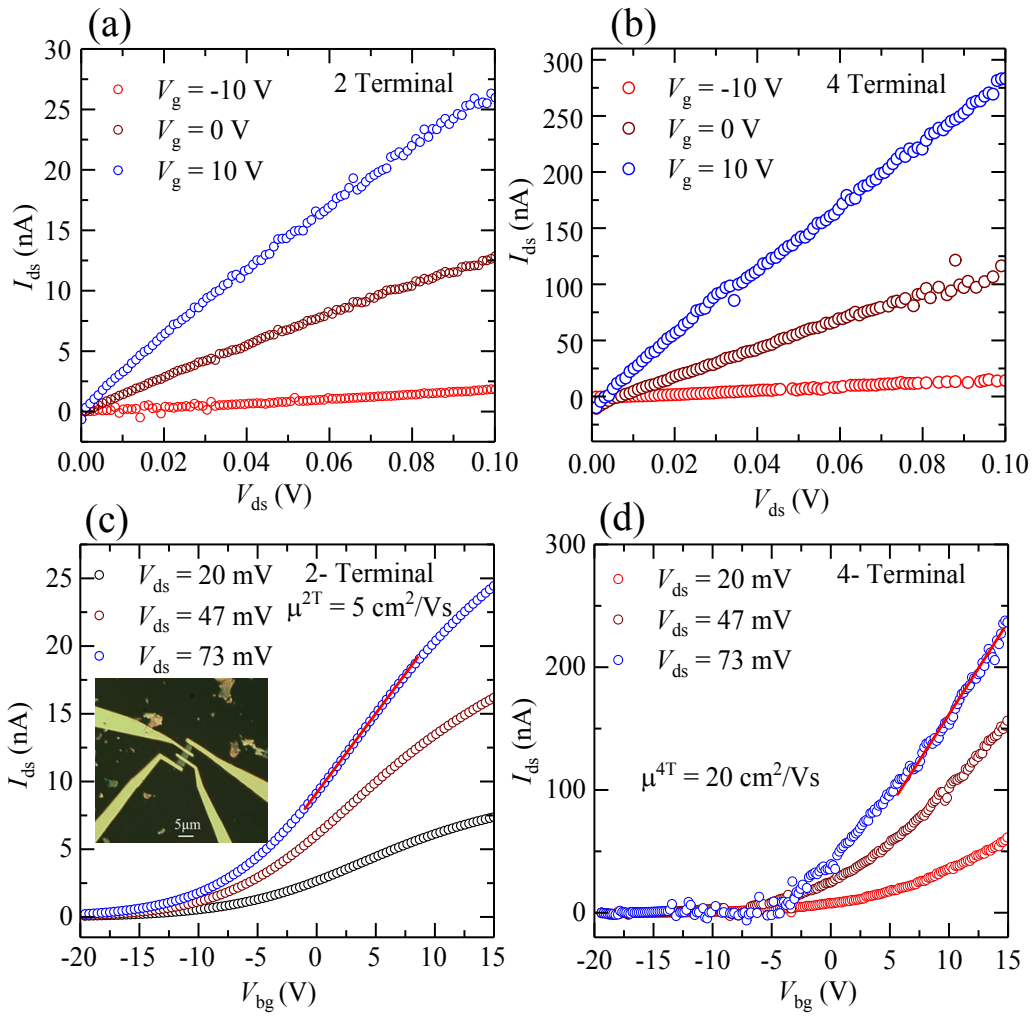

Figure S5: Display the drain-to-source current as a function of applied source-drain voltage measured using (a) 2-terminal and (b) 4-terminal configurations. (c) and (d) display the drain-source current as a function of applied gate voltage at V_{ds} = 20 mV, 47 mV and 73 mV measured using 2- and 4-terminals, respectively. The red line for V_{ds} = 73 mV is the linear fit to the experimental data used to extract the slope to estimate the mobility of the device. Inset of figure (c) shows the optical images of the FET device # 2 with channel length L = 20.3 µm, l = 6.9 µm and width W = 5.4 µm. The thickness of the MoS_2 used here is 15 nm obtained from the AFM height image.

Figure S5 (a) and S5 (b) display the I_{ds} as a function of V_{ds} measured in 2- and 4-terminals, respectively. The data shows a linear dependency in agreement with the results obtained for device #1 presented in the main text. The current measured in 4-terminal method is an order of magnitude than those obtained using the 2-terminal method. The FET transport properties are depicted in Figure S4 (c) and S4 (d) where the FET shows OFF in negative gate bias and ON while sweeping to the positive gate voltage, which indicates this to be a n-type MoS_2 transistor. The extracted charge carrier mobility values for 2- and 4-terminal measurements are 5 cm^2/Vs and 20 cm^2/Vs respectively.

6. Photoconductivity under white light illumination

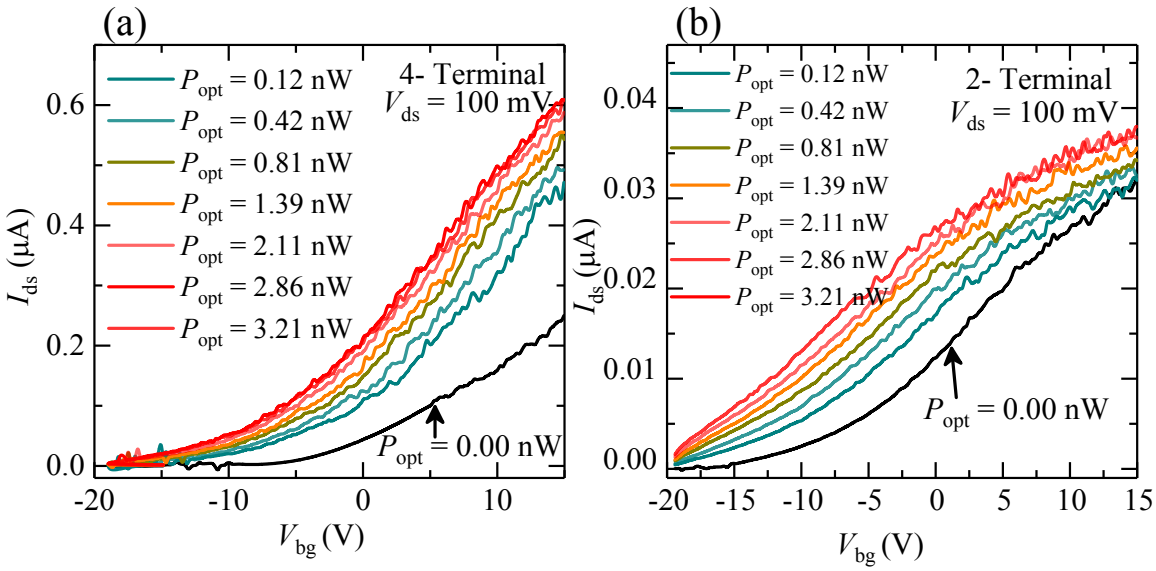

Figure S6: (a) and (b) are drain-to-source current as a function of applied gate voltage for 4-terminal and 2-terminals respectively, under white light illumination at different power.

Figure S6 shows the current measured from the device as a function of gate voltage while illuminated by a white light source at the given power as described in the main text. The measured current increases with increasing optical power. The current measured at P_{opt} = 0 nW is called the dark current (I_{dark}). The photocurrent (I_{ph}) was extracted by subtracting I_{dark} from the I_{ds} value ($I_{ph} = I_{ds} - I_{dark}$), which was used to estimate the responsivity of the device discussed in later section. The photocurrent measured in 4-terminal configuration shows much higher values than those measured using 2-terminal configurations.

7. Photoresponsivity (*R*)

We calculated the photoresponsivity using the formula $R = I_{ph}/P_{opt}$, where P_{opt} is the optical power illuminated on the channel area of the device. The responsivity measured in 4-terminal configuration shows values an order of magnitude higher than those measured in 2-terminal configuration, which agrees well with the device # 1 described in the main text.

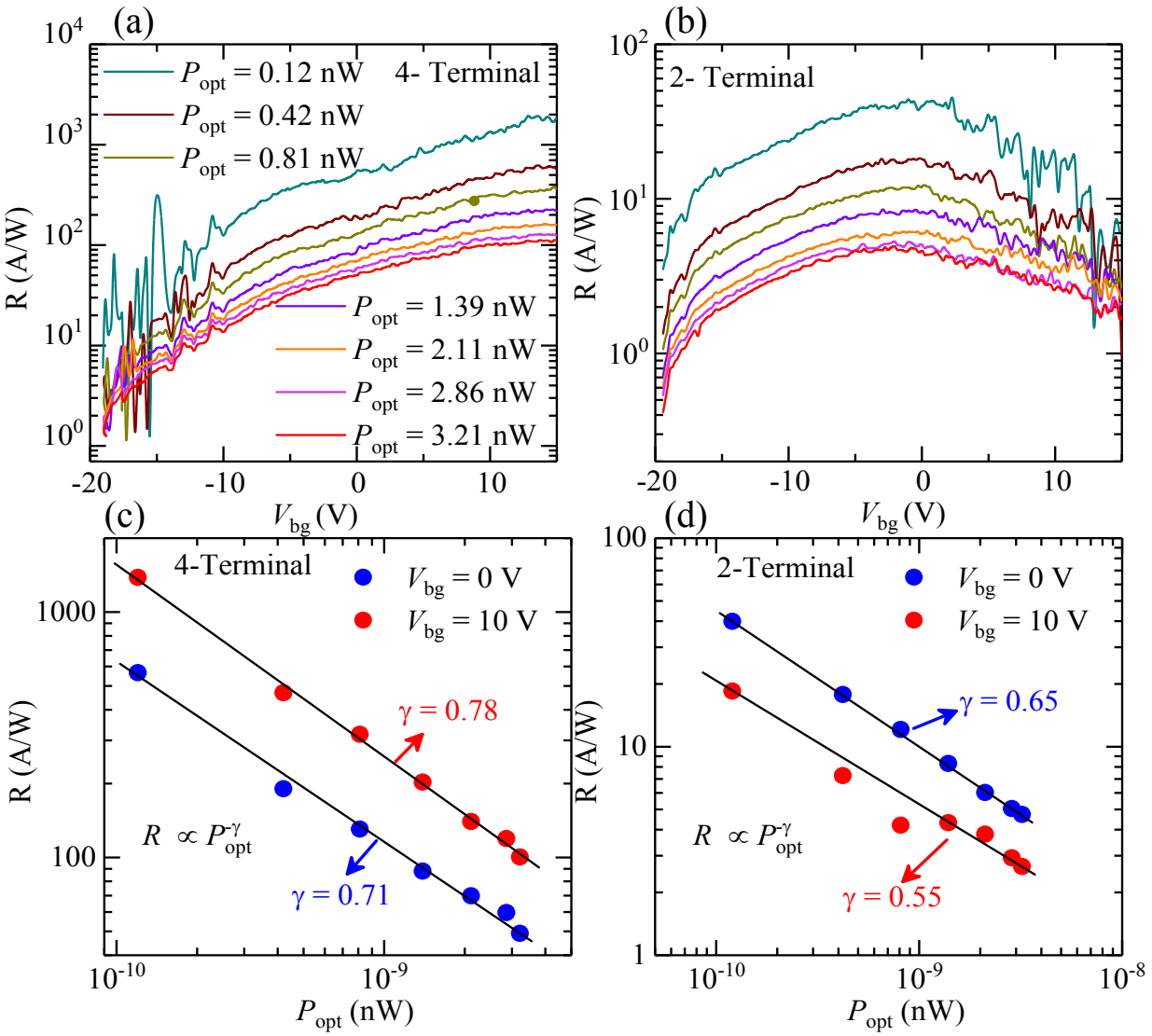

Figure S7: (a) and (b) display the responsivity measured in 4-terminal and 2-terminal configurations respectively as a function of applied gate bias while illuminating with white light with different optical power. (c) and (d) shows the logarithmic plot of the responsivity as a function of optical power at fixed gate voltages 0 V and 10 V for 4-terminal and 2-terminal measurements, respectively.

The responsivity of device #2 as a function of gate voltage measured in 4-terminal shows similar trend as device #1 described in main text, Fig. 3 (d). The responsivity increases with applied gate voltage and saturates when the transistor is in the ON state. The responsivity measured in 2-terminal configuration shows broad peak like feature as measured in device # 1 (main text Fig. 3 (c)). The responsivity values decrease with increasing illuminating optical power, which is depicted in the Figure S7 (c) and S7 (d).

8. Contact resistance (R_c) vs V_{bg} and P_{opt}

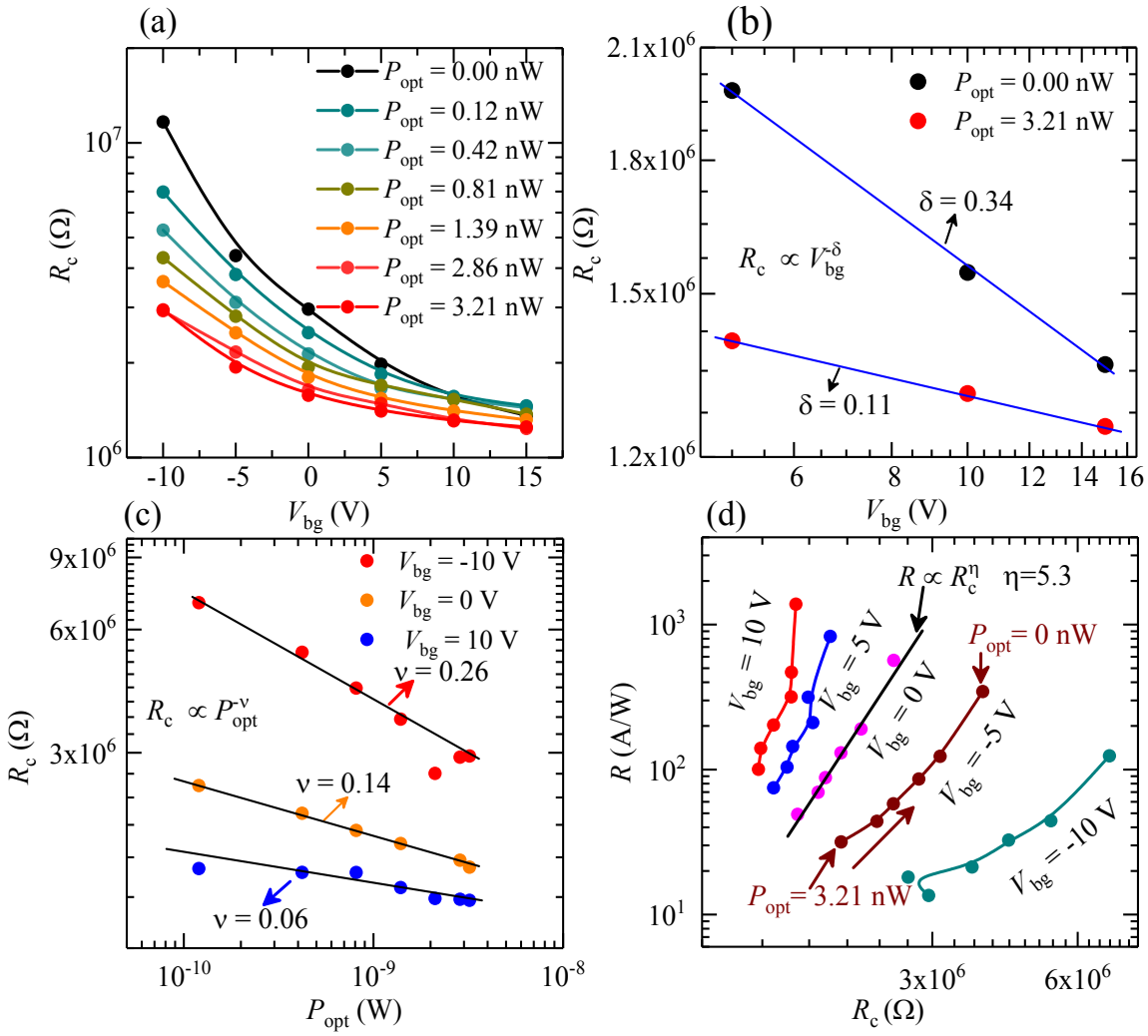

Figure S8: (a) Shows the contact resistance as a function of gate voltage at different applied optical power. (b) Log-log plot of R_c vs V_{bg} at P_{opt} = 3.21 nW and without light illumination. (c) R_c as a function of P_{opt} at V_{bg} = -10 V, 0 V and 10 V. (d) Shows the responsivity measured in 4-terminal method as a function of contact resistance in log-log plot, which shows the direct relationship between responsivity and contact resistance at fixed gate voltages. Each line corresponds to a constant V_{bg} but power varies as indicated (arrow on V_{bg} = -5 V) for the curve at V_{bg} = -5V.

The contact resistance displayed in Figure S8 (a) shows an exponential decrease of R as a function of V_{bg}. The change in R_c is larger at low gate voltage. Furthermore, R_c is greatly influenced by the intensity of the optical power. At a low gate voltage, (V_{bg} = -10 V or OFF state of the transistor), less charge carriers accumulated in the channel and when under illumination, many electron-hole pairs are created by the absorption of photon. This electron-hole pair generation increases as a function of optical power resulting in a large current being conducted through the channel which reduces R_c significantly. At high enough positive gate voltage (V_{bg} > 5 V) or when the FET was in its ON state, R_c does not vary significantly. When the FET is in its ON state, most of the carriers accumulate at the interface, thus illuminating the device or varying the optical power does not change the number of electron-hole pairs created and, thus change in R_C is minimum.

In order to further understand the influence of the contact resistance in our results, we plotted R_c as a function of V_{bg} in power law form $R_c \propto V_{bg}^{-\delta}$ at fixed P_{opt} in Figure S8 (b). The data fits well with a power law form, in which the exponent δ varies from 0.11 (for P_{opt} = 3.21 nW) to 0.34 (for P_{opt} = 0 nW). We also plotted R_c as a function of P_{opt} at fixed gate voltage in Figure S8 (c) similar to the Fig. 4 (b) described in the main text and fitted again with a power law of the form $R_c \propto P_{opt}^{-\upsilon}$. The exponent υ varies from 0.06 (at V_{bg} = 10 V) to 0.26 (at V_{bg} = -10 V). These two power law fits explain how the contact resistance is affected by the gate voltage and illuminated optical power. The photoresponsivity, also power-law dependent with P_{opt}, $R \propto P_{opt}^{-\gamma}$ at fixed V_{bg} and already discussed in Figure S6. From these two power law relations $R \propto P_{opt}^{-\gamma}$ and $R_c \propto P_{opt}^{-\upsilon}$ at fixed gate voltage, we extracted the direct relation between photoresponsivity (R) and R_c, which

yields $R \propto R_c^{\frac{\gamma}{\nu}} = R \propto R_c^{\eta}$, where $\eta = \frac{\gamma}{\nu}$. We have plotted R as a function of R_c in logarithmic scale (Figure S8 (d)) and fitted one of the data sets at V_{bg} = 0V, which yields $\eta = 5.3$. This is very close to the calculated value using the relation $\frac{\gamma}{\nu} = 5.1$. These data show how the contact resistance influences the photoresponsivity of the photodetectors.

Reference:

1. Z. Yin, H. Li, H. Li, L. Jiang, Y. Shi, Y. Sun, G. Lu, Q. Zhang, X. Chen, and H. Zhang, *ACS nano* 2012, **6**, 74-80.
2. W. Choi, M. Y. Cho, A. Konar, J. H. Lee, G.-B. Cha, S. C. Hong, S. Kim, J. Kim, D. Jena, J. Joo, and S. Kim, *Adv. Mater.* 2012, **24**, 5832- 5836.
3. O. Sanchez, D. Lembke, M. Kayci, A. Radenovic, and A. Kis, *Nat Nanotechnol* 2013, **8**, 497-501.
4. D.-S. Tsai, K.-K. Liu, D.-H. Lien, M.-L. Tsai, C.-F. Kang, C.-A. Lin, L.-J. Li, and J.-H. He, *Acs Nano* 2013, **7**, 3905- 3911.
5. Y. T. Lee, J.-H. Kang, K. Kwak, J. Ahn, H. T. Choi, B.-K. Ju, S. H. Shokouh, S. Im, M.-C. Park, and D. K. Hwang, *ACS Photonics* 2018, **5**, 4745- 4750.
6. S. Lee, Y. Park, G. Yoo, and J. Heo, *Appl. Phys. Lett.* 2017, **111**, 223106 (1-5).
7. Y. Xie, B. Zhang, S. Wang, D. Wang, A. Wang, Z. Wang, H. Yu, H. Zhang, Y. Chen, M. Zhao, B. Huang, L. Mei, and J. Wang, *Adv. Mater.* 2017, **29**, 1605972 (1-6).
8. D. Kang, M. Kim, J. Shim, J. Jeon, H. Park, W. Jung, H. Yu, C. Pang, S. Lee, and J. Park, *Adv. Funct. Mater.* 2015, **25**, 4219-4227.
9. J. Kwon, Y. K. Hong, G. Han, I. Omkaram, W. Choi, S. Kim, and Y. Yoon, *Adv. Mater.* 2015, **27**, 2224-2230.
10. W. Tang, C. Liu, L. Wang, X. Chen, M. Luo, W. Guo, S. Wang, and W. Lu, *Appl. Phys. Lett.* 2017, **111**, 153502 (1-4).
11. K. Dominik, and G. Konstantatos, *Nano lett.* 2015, **15**, 7307-7313.
12. S. Qiao, R. Cong, J. Liu, B. Liang, G. Fu, W. Yu, K. Ren, S. Wang, and C. Pan, *J. Mater. Chem. C* 2018, **6**, 3233-3239.

13. L. Wang, J. Jie, Z. Shao, Q. Zhang, X. Zhang, Y. Wang, Z. Sun, and S. Lee, *Adv. Funct. Mater.* 2015, **25**, 2910-2919.
14. Y. Li, C. Xu, J. Wang, and L. Zhen, *Sci. Rep.* 2014, **4**, 7186 (1-8).
15. K. Roy, M. Padmanabhan, S. Goswami, T. P. Sai, G. Ramalingam, S. Raghavan, and A. Ghosh, *Nat. Nanotechnol.* 2013, **8**, 826-830.
16. H. Xu, J. Wu, Q. Feng, N. Mao, C. Wang, and J. Zhang, *Small* 2014, **10**, 2300-2306.
17. L. Tu, R. Cao, X. Wang, Y. Chen, S. Wu, F. Wang, Z. Wang, H. Shen, T. Lin, P. Zhou, X. Meng, W. Hu, Q. Liu, J. Wang, M. Liu, and J. Chu, *Nat. Commun.* 2020 11:101, https://doi.org/10.1038/s41467-019-13769-z .
18. C. Lee, H. Yan, L. E. Brus, T. F. Heinz, J. Hone and S. Ryu, *ACS Nano* 2010, **4**, 2695-2700.